Progressive Failure Analysis Using Global-Local Coupling Including Intralaminar Failure and Debonding

Margarita Akterskaia*, Eelco Jansen†, Stephen R. Hallett‡, Paul M. Weaver§ and Raimund Rolfes¶
Leibniz Universität Hannover, Institute of Structural Analysis, 30167 Hannover, Germany
University of Bristol, Bristol Composites Institute (ACCIS), BS81TR Bristol, UK
Bernal Institute, University of Limerick, Castletroy, Ireland

Composite laminate stiffened panels are often used in aircraft fuselage design because of their favourable properties. To assess the failure load of these thin-walled structures and to exploit their reserves, a reliable simulation capability for their postbuckling behaviour is often necessary. To perform a realistic failure analysis and to accurately detect final collapse, material degradation should be considered. Global-local approaches are computationally efficient techniques to perform a progressive failure analysis and to examine localized damaged areas in detail. In this paper, a two-way coupling global-local approach is presented, including a combination of different damage modes, such as matrix cracking, fiber damage and skin-stringer debonding. An accurate exchange of information concerning the damage state between global and refined local models is performed. From the global to the local model, the displacements are transferred through a submodeling procedure. Afterwards, the degraded material properties obtained from the local model analysis are returned to the global model with a special mapping technique that accounts for the different mesh sizes at the two levels. The two-way coupling procedure is applied to the progressive failure analysis of a one-stringer composite panel loaded in compression. Finally, the numerical results of the procedure are compared with experimental results.

I. Nomenclature

A	=	area
$\mathbf{C}$	=	material stiffness matrix
d	=	damage variable for cohesive element
d_f	=	damage variable for the fibre degradation by Linde
d_m	=	damage variable for the matrix degradation by Linde

*Research Associate, Institute of Structural Analysis, Leibniz Universität Hannover, Germany.
†Senior Faculty Member, Institute of Structural Analysis, Leibniz Universität Hannover, Germany.
‡Professor, Bristol Composites Institute, (ACCIS), University of Bristol, UK.
§Professor, Bristol Composites Institute, (ACCIS), University of Bristol, UK and Bernal Institute, University of Limerick, Castletroy, Ireland.
¶Professor, Institute of Structural Analysis, Leibniz Universität Hannover, Germany.

δ	=	maximum relative displacement
E	=	Young's modulus
F	=	force
f_f	=	fibre failure condition for Linde criterion
f_m	=	matrix failure condition for Linde criterion
G	=	shear stiffness
G_f	=	fracture energy of fibre
G_m	=	fracture energy of matrix
G_{Ic}	=	total critical energy release rate in mode I
G_{IIc}	=	total critical energy release rate in mode II
G_I, G_{II}, G_{III}	=	energy release rates in mode I, II and III
$\mathbf{K}$	=	interface stiffness matrix
K_0	=	initial interface stiffness
L	=	length
L_C	=	characteristic element length
S_A	=	axial shear strength
S_T	=	transverse shear strength
t	=	thickness
w	=	width
X_C	=	longitudinal compressive strength
X_T	=	longitudinal tensile strength
Y_C	=	transverse in-plane compressive strength
Y_T	=	transverse in-plane tensile strength

II. Introduction

The extensive use of fiber-reinforced composite laminates in the aircraft application for light-weight structures during the last decades is explained by their excellent material properties such as high strength and stiffness ratios. However, composite structures demonstrate great advantages, the numerical assessment and experimental validation involve high costs. A finite element global-local coupling approach is a widely applied methodology in failure analysis of structures that aims at reducing computational efforts on the one hand and at accurately examining critical areas where damage occurs on the other.

A. Global-Local Coupling Methods

Within the context of coupling approaches, one-way and tight coupling methods prevail. One-way coupling is a term used to describe a transfer of information in one direction between separated models, i.e. from the global to the local level or visa versa. Tight coupling means that global and local models are not separated and systems of equations are solved simultaneously. An overview of these methods can be found in Hühne et al. [1]. Certain two-way methods are available that can treat global and local models separately. The multiscale projection method by Löhnert and Belytschko [2] simulated fracture and crack propagation using XFEM to investigate the effect of macrocracks and microcracks interactions leading to damage. The adaptive progressive damage modelling technique by Labeas et al. [3] was used for the prediction of damage initiation and evolution in composite structures. Their approach combines a progressive damage modelling technique with the submodeling method. The homogenization-based iterative two-way multiscale approach by Chrupalla et al. [4] accounted for the effects of local damage on the global behavior of composite structures. The main difference between the aforementioned approaches is the way the degraded properties are transferred back from the local to the global level. An efficient local-global transfer technique for composite structures proposed by Hühne et al. [1], which includes matrix and fiber failure, was based on calculation of effective material properties and is extended in the current research. The present technique is different from the ones used in other works. A more accurate homogenization scheme is used than the simplified procedure of averaging the local engineering constants performed by Labeas et al. [3]. Another advantage of the present approach is that it is non-intrusive in the sense that it can be directly combined with standardly available commercial finite element codes.

Skin-stringer debonding in composite panels has been considered by several authors. A loose one-way coupling analysis was performed by Reinoso et al. [5]. In this approach, information was transferred from the global to the local level and cohesive elements were utilized for the local model. Orifici et al. [6] performed global-local analysis with ply degradation and a method for capturing interlaminar crack growth based on multi-point constraints controlled using the Virtual Crack Closure Technique. The creation of the local models was based on monitoring a strength-based criterion in the skin–stiffener interface. An optimization technique employing a genetic algorithm was proposed by Faggiani and Falzon [7], which aimed at minimizing debonding damage in the postbuckling regime of stiffened panels by optimizing the laminate stacking sequence. A global-local method was applied in the analysis of a panel with I-shaped stiffeners in order to make the application of the optimization procedure feasible. The non-intrusive global-local technique by Gendre et al. [8] examined separately a global linear model of the whole structure and a local nonlinear submodel representing the critical area. After each iteration loop, a residual force vector was calculated from the difference between global and local reaction forces at the border of these models. This load vector was applied to the nodes of the global model in order to provoke the deformation of the global model, transferring the influence of the local nonlinearities. Vescovini et al. [9] performed a one-way coupling analysis. Shell elements were used for the global and local models, while cohesive elements were applied to model interface layer at the local level. The main limitations

of existing coupling approaches are associated with their efficiency in detecting critical areas at the global level and their accuracy in information exchange between global and local levels, in particular their capability to account for mutual interaction. In the current work, a transition of degraded properties from the local to the global level assures that damage propagation is appropriately represented within a progressive failure analysis at the global level.

B. Developed Global-Local Two-way Loose Coupling Approach

In the global-local coupling procedure for composite stiffened panels developed by Hühne et al. [1] and enhanced later by Akterskaia et al. [10], intralaminar damage (fibre and matrix damage) was analysed. Akterskaia et al. subsequently developed a new global-local approach for progressive failure in stiffened panels with skin-stringer separation [11]. In the present paper, the limitation of the previous works where only one type of damage was considered is overcome. The debonding damage between skin and stringer and intralaminar damage are examined together, so that various important failure modes are incorporated in the approach. It is important to note that matrix and fiber damage as well as debonding are principal failure modes as observed during experiments conducted for laminated stiffened panels [12]. Skin-stringer separation is recognized as a crucial damage mode that can lead either to a final collapse of the structure, or in the case of good bonding between the skin and the stringer, it could trigger other damage mechanisms, such as delaminations in adjacent layers and fiber failure in the stringer [5], [13], [14]. The main idea of the loose coupling procedure proposed in the current work [10], [11] is demonstrated in Fig. 1, where the procedure is shown only for the case of skin-stringer debonding.

The flowchart of the two-way loose coupling procedure [1] is shown in Fig. 2. A global analysis is conducted, followed by local model calculations and local-global transfer of reduced properties. Afterwards the global analysis is repeated to check whether the stress redistribution induced by degraded material properties results in the appearance of new critical areas or an extension of existing ones which is shown in the flowchart in the diamond called "New local damage?". The global-local procedure is performed until no new intralaminar damage initiation or no new skin-stringer separation onset is detected at the prescribed displacement level under consideration. When this “iteration loop” is completed, the load at the global level is increased and thereby the next “coupling loop” is started. The procedure is performed until final failure of the structure occurs. The proposed global-local method was developed for structures experiencing localized damage. Hence, an assumption has been formulated stating that limited amount of coupling loops are required to reach a state of the final failure. In the present paper, this procedure is applied for the case, in which skin-stringer debonding and intralaminar damage occur simultaneously, as happens in realistic experimental tests.

The main advantage of the presented approach is that no preliminary knowledge is required about the location and the size of the intralaminar damage and the skin-stringer debonding as the damage initiation is monitored at the global level. Another important aspect is the exchange of the damage information from the local to the global level through the reduced material properties which allows for the performing of the progressive failure analysis until the final collapse.

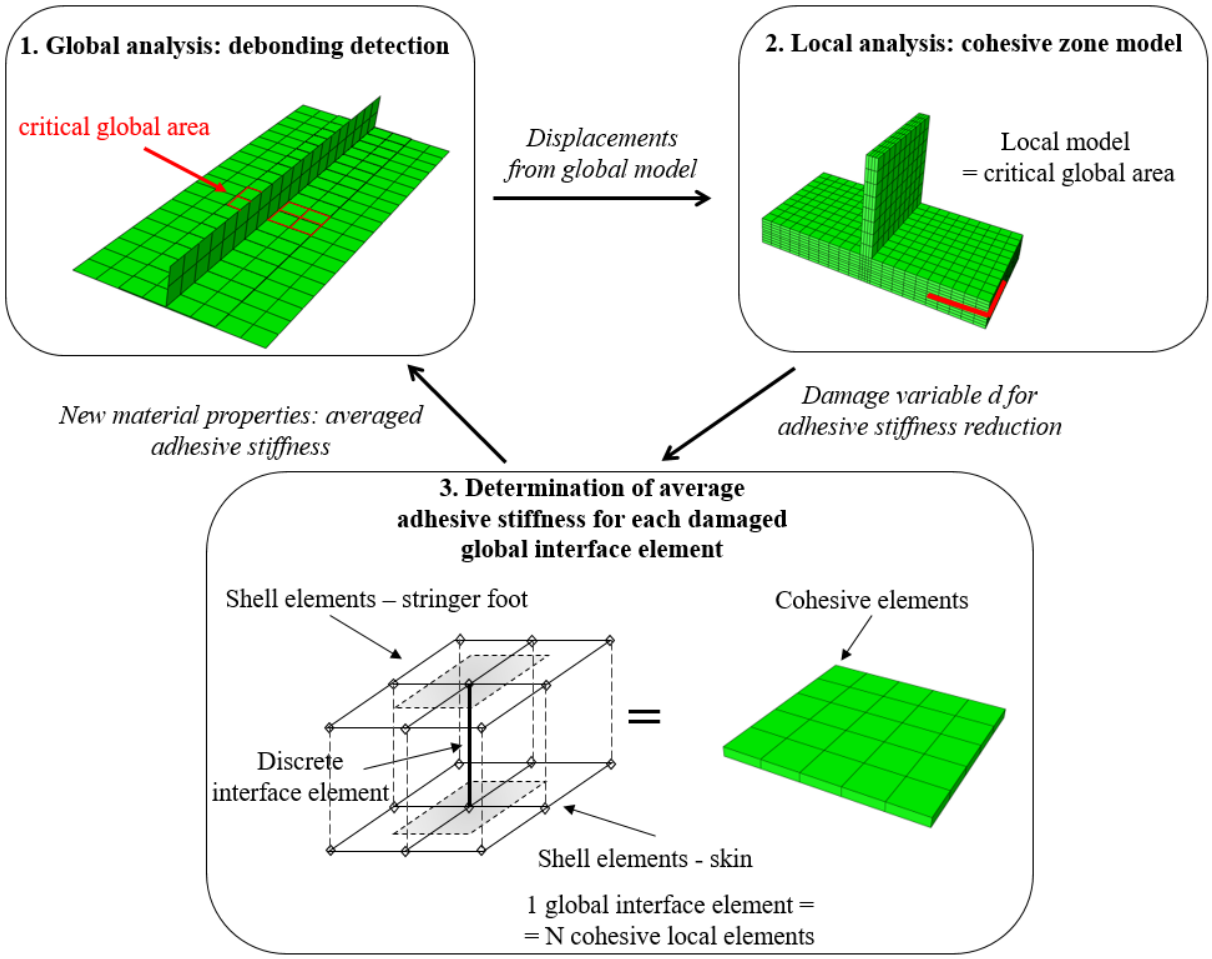

Fig. 1 Two-way loose coupling procedure for skin-stringer debonding: application to a one-stringer stiffened panel. The grey area around connector element corresponds to the nodal area of this connector element

III. Detailed Methodology: Two-Way Loose Coupling Approach with Interlaminar and Intralaminar Failure

The progressive failure analysis (using the commercial finite element (FE) software Abaqus) is carried out until global failure of the structure takes place. The skin and the stringer of the panel in the global model are represented by 4-node laminated shell elements using reduced integration (S4R elements). The adhesive layer is regarded as a structural connection and was modelled with connector elements of Cartesian type available in Abaqus. These elements were selected, since the prediction of debonding initiation in the adhesive layer requires knowledge of the normal and shear stress, whereas application of 3D solid elements is not recommended because of their inappropriate aspect ratio. The model at the global level is used to identify the areas where matrix or fibre failure are expected to occur by applying the Linde criterion [15], which stems from the Puck criterion and distinguishes between fibre and matrix damage as well as between compressive and tensile stresses. The material damage model performs a gradual degradation of material properties using the fracture energies of fibre and matrix. In the following, X_T and X_C denote the longitudinal tensile

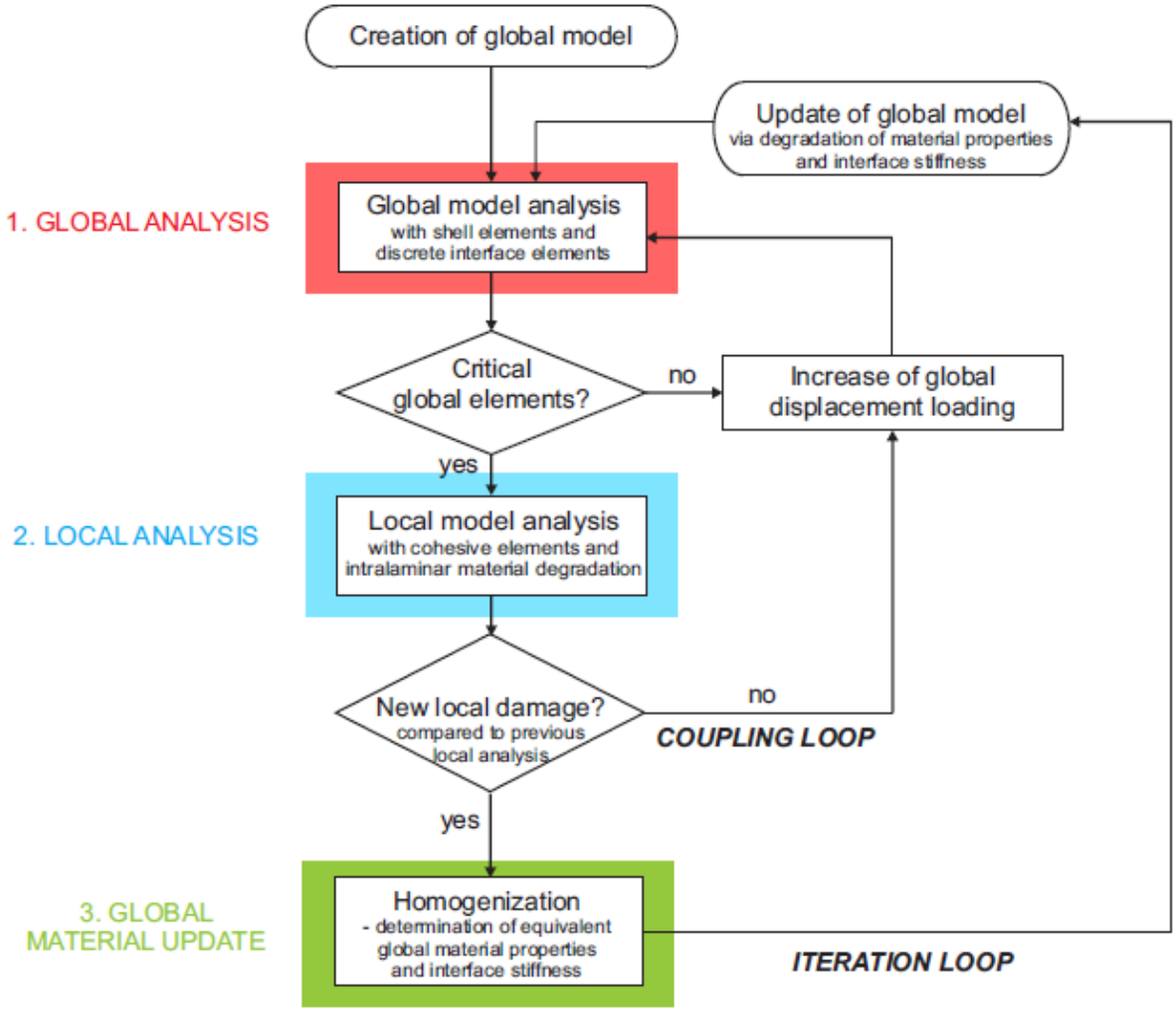

Fig. 2 Flowchart of two-way loose coupling procedure for intralaminar failure and skin-stringer debonding.

and compressive strength, respectively, and Y_T and Y_C are the transverse in-plane tensile and compressive strength, respectively, whereas S_A is the axial shear strength and C_{ij} are the components of the stiffness matrix. Damage initiates in the matrix when the index f_m exceeds the failure strain perpendicular to the fiber direction in tension and calculated as Y_T/C_{22} and fibre damage occurs when the index f_f exceeds X_T/C_{11} which is the failure strain in the fiber direction in tension, see Eqs. 1 and 2:

$$f_m = \sqrt{\frac{Y_T}{Y_C}(\epsilon_{22})^2 + \left(Y_T - \frac{Y_T^2}{Y_C}\right)\frac{\epsilon_{22}}{C_{22}} + \left(\frac{Y_T}{S_A}\right)^2 \epsilon_{12}^2} > \frac{Y_T}{C_{22}} \tag{1}$$

$$f_f = \sqrt{\frac{X_T}{X_C}(\epsilon_{11})^2 + \left(X_T - \frac{X_T^2}{X_C}\right)\frac{\epsilon_{11}}{C_{11}}} > \frac{X_T}{C_{11}} \tag{2}$$

where the strain components ϵ_{ij} correspond to the local material coordinates related to the orientation of the fibers, index *1* refers to the fibre direction, whereas index *2* (in-plane) and index *3* (out-of-plane) refer to the transverse directions. The damage parameters d_m and d_f introduced by Linde correspond to the partial matrix and fiber degradation:

$$d_m = 1 - \frac{Y_T}{f_m} e^{-\left(\frac{C_{22} Y_T (f_m - Y_T) L_c}{G_m}\right)} \tag{3}$$

$$d_f = 1 - \frac{X_T}{f_f} e^{-\left(\frac{C_{11} X_T (f_f - X_T) L_c}{G_f}\right)} \tag{4}$$

The characteristic element length L_C is used to reduce the mesh dependency of the degradation model. The matrix and fiber strengths are G_m and G_f, respectively. The undamaged elasticity tensor is C_{ij} (where i,j=1,6). The effective elasticity tensor C_d used by Linde [15] is defined as:

$$\mathbf{C} = \begin{pmatrix} (1-d_f)C_{11} & (1-d_f)(1-d_m)C_{12} & (1-d_f)C_{13} & 0 & 0 & 0 \\ & (1-d_m)C_{22} & (1-d_m)C_{23} & 0 & 0 & 0 \\ & & C_{33} & 0 & 0 & 0 \\ & & & (1-d_f)(1-d_m)C_{44} & 0 & 0 \\ & symmetric & & & C_{55} & 0 \\ & & & & & C_{66} \end{pmatrix} \tag{5}$$

It is worth mentioning that the presented global-local strategy is not restricted to the particular intralaminar failure criterion used and other criteria such as LaRC04 by Pinho et al. [16] or developed later by Pinho et al. [17] could be applied. A good overview of existing failure criteria and their comparison have been performed during the effort of three stages of World Wide Failure Exercise (WWFE), see Hinton et al. [18], Kaddour and Hinton [19], Kaddour et al. [20] and Kaddour et al. [21]. Material degradation models are reviewed in [22] and more recently in [23]. However, the particular choice of the Linde criterion is explained by the aim to obtain reliable results at a relatively low computational costs with an accurate material model, but also with a reasonably simple model that is not excessively demanding in terms of material model parameters required. The Linde criterion is an appropriate criterion for our current purposes. The relative simplicity of the implementation and the possibility of combining it with the material degradation model by Linde are convenient. It is noted, that other failure criteria can also be used within the current implementation of the global-local framework. Since the criterion distinguishes between matrix and fibre failure, it retains the possibility of a validation with experimental results.

The regions of the interface layer where the onset of debonding between skin and stringer may take place are

determined by means of a quadratic stress criterion, expressed by the following relation:

$$\left(\frac{<\sigma_{33}>}{N_{max}}\right)^2 + \left(\frac{\sigma_{13}}{S_{max}}\right)^2 + \left(\frac{\sigma_{23}}{T_{max}}\right)^2 \geq 1 \tag{6}$$

Here <. . . > represents Macauley brackets operator, σ_{33} is a stress in the pure normal mode, σ_{13} and σ_{23} are nominal stresses acting in the first and second shear directions and N_{max}, S_{max}, T_{max} are the maximum corresponding stresses. The normal and two transverse shear stresses σ_{33} and σ_{13}, σ_{23} respectively are calculated based on the total forces:

$$\sigma_{i3} = \frac{F_i}{A_{el}}, \quad i = 1, 2, 3 \tag{7}$$

where F_i is a force and index i denotes 1- longitudinal, 2- transverse and 3- normal axis respectively, A_{el} is an area of applied force. A_{el} is equal to the full in-plane area of the shell element for interior connectors or to half of this area corresponding to the case when connectors tie the edges. There are also connectors applied to the corner nodes of the panel at both edges respectively. However, these corners do not represent regions of interest and, hence, they are not checked for the damage initiation.

After completion of the global analysis, the required number of local models is created based on the information about the size and the location of critical areas determined by the failure initiation criteria discussed earlier. The detailed model with refined mesh density at the local level allows for considering the influence of the damaged region at the global level. An advantage of interface cohesive elements technique over another common method, the Virtual Crack Closure Technique (VCCT), is their ability not only to observe the evolution of the damage through the interface, but also to predict the onset of the layer separation. These elements have already been successfully applied by other researchers [24], [25]. However, preliminary studies are required related to the accuracy of the mesh refinement, since a higher number of cohesive elements compared to the structural elements is needed in order to ensure reliable results [5], [26]. In the present study, the evolution of the debonding is assumed to be described through the Benzeggagh and Kenane fracture criterion [27] extended to 3D cases. The mixed mode critical energy release rate G_c is supposed to be equal to the area under the curve in the traction – separation diagram, see Fig. 3, and is calculated by:

$$G_c = G_{Ic} + (G_{IIc} - G_{Ic}) \left(\frac{G_{II} + G_{III}}{G_I + G_{II} + G_{III}}\right)^{\eta} \tag{8}$$

where G_{Ic} and G_{IIc} are mode I and II critical energy release rates and G_I, G_{II}, G_{III} are single mode energy release rates corresponding to fracture modes I, II and III and their sum is the total energy release rate. The parameter η is determined empirically [27] and is assumed to be 2.284 [24].

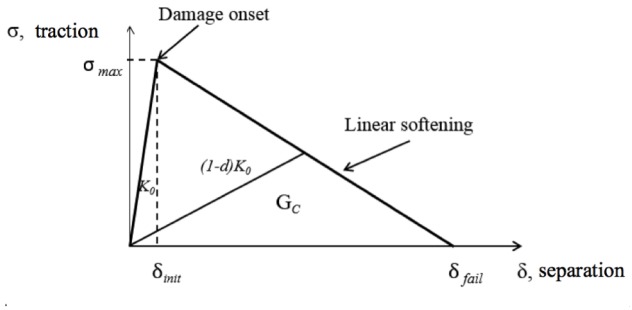

Fig. 3 Bilinear traction-separation law.

The initial stiffness of each discrete interface element is defined as follows:

$$K_0 = \frac{EA}{t} \tag{9}$$

where E is the Young's modulus of the corresponding interface material, A and t are in-plane nodal area and thickness in the normal direction of the interface element, respectively.

The linear degradation of the adhesive element stiffness is described by:

$$K_{eff} = (1 - d)K_0 \tag{10}$$

where the scalar parameter d varies from 0 for an undamaged element to 1 for a complete crack opening and K_0 is the initial stiffness. The intralaminar material properties of the skin and the stringer are degraded according to the material degradation model discussed in [1]. Averaged local stiffness was proposed to be calculated [11] for each area that corresponds to one connector element:

$$K_{local} = \frac{\sum_{i=1}^{N} K_{local,i}}{N} = \frac{\sum_{i=1}^{N} (1 - d_i) K_{local,0}}{N} = K_{local,0} \left(1 - \frac{\sum_{i=1}^{N} d_i}{N} \right) \tag{11}$$

where N is the number of local continuum interface elements corresponding to one global discrete interface element. Afterwards, the multiplication coefficient of the right term that is based on the averaged damage variable parameter d is used to obtain the degraded global interface stiffness:

$$K_{global_j} = K_{global_j,0} \left(1 - \frac{\sum_{i=1}^{N} d_i}{N} \right), \quad j = 1..N_{global} \tag{12}$$

where N_{global} is the number of global adhesive elements.

This approach allows an independent calculation of the multiplication coefficient for each global element. It is also important to note that only those global elemental stiffnesses are degraded during the next coupling loop that correspond to the local cohesive elements in the softening regime. Other global adhesive elements keep their initial stiffness.

The required number of coupling loops described in Fig. 2 is carried out until the global panel failure occurs. Comparisons are conducted first with a full reference model with a mesh size, that is comparable to the local model, where solid elements are used for the skin and the stringer and cohesive elements are applied for the interface layer. Secondly, the numerical predictions of the global-local method are compared to the experimental results of a one-stringer panel.

Another interlaminar damage mechanism such as delamination of the adjacent layers is not considered within the presented approach. On the one hand, this type of damage was not reported as critical to the structural collapse as the final failure in stiffened panels under compression usually takes place due to the initiation and growth of matrix damage and skin-stringer separation finishing by final fiber failure. On the other hand, within the current framework of the global-local method it is not directly possible to predict the delamination onset with conventional elements at the global level. However, in cases when it is known in advance at which position a delamination is expected to occur, the initial model could make use of stacked shell elements and our current debonding procedure could be used.

IV. Application of the Two-Way Loose Coupling Procedure to a One-Stringer Composite Panel

First, the method is applied to a stiffened panel with one T-shaped stringer. This panel is demonstrated in Fig. 4, geometrical and material characteristics are listed in Table 1 and Table 2, respectively. The material "1-direction" corresponds to the longitudinal axis of the panel. The unidirectional layers are of 0.25 mm thickness each with a symmetric composite layup $[0;90]_s$. Progressive damage was examined under the following boundary conditions: a fully clamped transverse edge is used and the opposite transverse edge is constrained in all directions except for the longitudinal direction, in which compressive load is imposed as prescribed displacement. Longitudinal edges are free to deform.

A. Reference Model

In order to evaluate the results of the coupling approach, a 3D reference model was created. Linear 8-nodes solid elements (C3D8) with a nominal element edge length of 1 mm were employed for modelling the skin and the stringer, one element per layer resulting in 4 elements through thickness. Non-zero thickness cohesive elements with bilinear traction-separation law replaced the connector elements in the adhesive area. The adhesive properties are summarized in Table 3. Four cohesive elements per side of one solid element were chosen after performing convergence studies to

Table 1 Geometry of stiffened composite panel.

Description	Value
Panel length, l (mm)	100
Panel width, w (mm)	40
Stringer width, b (mm)	20
Stringer height, h (mm)	8
Laminate thickness, t_{skin}, t_{blade} (mm)	1
Adhesive thickness, t_{adh} (mm)	0.2

Table 2 Material data for composite and adhesive.

Stiffness properties	Value
Young's modulus in 1-direction, E_{11} (GPa)	146.5
Young's modulus in 2-direction, E_{22} (GPa)	9.7
Shear modulus in 12-plane, G_{12} (GPa)	5.1
Poisson's ratio, ν_{12}	0.28
Tensile failure stress in 1-direction, X_T (MPa)	2583
Compressive failure stress in 1-direction, X_C (MPa)	1483
Tensile failure stress in 2-direction, Y_T (MPa)	92
Compressive failure stress in 2-direction, Y_C (MPa)	270
Shear failure stress in 12-plane, S_A (MPa)	106
Fracture energy of fiber, G_f (N/mm)	12.5
Fracture energy of matrix, G_m (N/mm)	1.0
Young's modulus of adhesive, E_{adh} (GPa)	3.0
Poisson's ratio of adhesive ν_{adh}	0.4

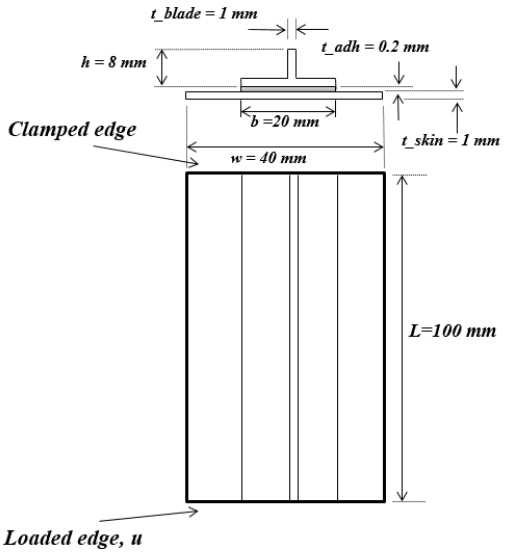

Fig. 4 Geometry of the tested one-stringer stiffened panel.

Table 3 Material data for cohesive elements, adhesive type FM300 from [6].

Cohesive element properties	Value
Interface element stiffness before the damage onset, K (N/mm^3)	10^6
Interfacial strength, mode I, τ_I (MPa)	61
Interfacial strength, mode II and III, τ_{II}, τ_{III} (MPa)	68
Fracture toughness, mode I, G_{Ic} (N/mm)	0.243
Fracture toughness, mode II and III, G_{IIc}, G_{IIIc} (N/mm)	0.514

estimate the minimum required number of cohesive and solid elements. The total number of elements was defined after the preliminary mesh convergence studies: 68,800 elements in total, from which 38,400 are cohesive elements. To connect different mesh sizes of the skin and the foot of the stringer to the larger number of adhesive elements, the Abaqus *TIE constraint was used, with special attention to the choice of the master and slave surface [5]. The master surface corresponds to a skin or a stringer surface, slave surfaces correspond to the cohesive elements.

The material degradation model by Linde [15] was implemented through the Abaqus user-defined material subroutine (UMAT) to account for intralaminar damage. Interlaminar damage was examined with cohesive elements with the bilinear traction-separation law. An imperfection with the shape of the first eigenmode obtained from the linear buckling analysis was applied, similar to the global analysis.

B. Global Model: Linear Elastic Material

The global model consists of 280 4-node shell elements of 5 mm nominal element edge size using reduced integration (Abaqus S4R elements). A user-defined material subroutine (UMAT) was utilized to define the global material properties

obtained from the local level calculations. An adhesive layer between the skin and the foot of the stringer was modelled with connector elements. The axial compressive displacement was applied to the transverse edge and a static nonlinear analysis in Abaqus Standard was performed. The first eigenmode was chosen to trigger the buckling deformation of the panel. For the post-processing of the global model results, two Python scripts were used. The first one was developed previously by Hühne et al. [1] to determine the critical global areas through the damage initiation criterion for matrix and fibre by Linde [28] discussed above. The same criterion is also applied to a local model. The second python script was developed with the goal of identification of critical regions due to the debonding onset by the quadratic stress criterion (Eq. 6) applied to the connector elements.

Four global-local coupling loops were performed with a consequent increase of the applied displacement: u=0.56 mm, 0.60 mm, 0.63 mm and 0.67 mm until the final failure was detected. An example of damaged areas detected during the global analysis of the first coupling step is demonstrated in Fig. 5. At the applied displacement of 0.56 mm, the post-processing tool detected the potential areas of matrix damage and debonding initiation between the skin and the stringer. Based on these critical regions, two local models were created, Local model 1 and Local model 2, respectively.

Coupling loop 1. Global model:
(a) matrix damage estimation
(b) debonding onset prediction, connector elements

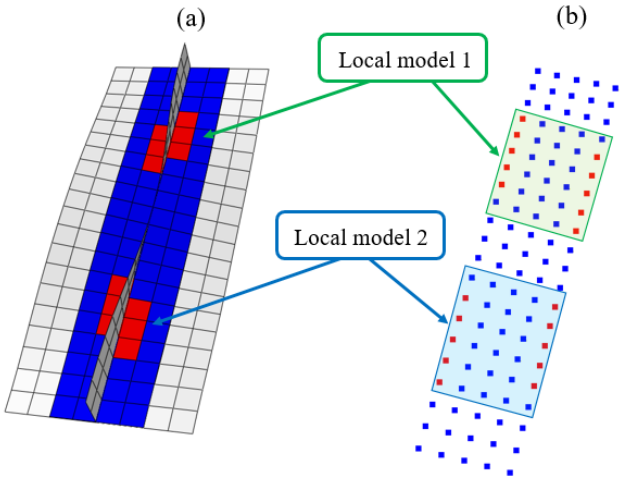

Fig. 5 Coupling loop 1, global level. Elements where damage onset was predicted are displayed in red. (a) First critical global areas related to matrix failure, (b) first critical connector elements.

C. Local Models: Material Non-Linearity and Cohesive Debonding

The local models are created automatically for the critical areas identified during the global simulation by using a MATLAB preprocessor. Input parameters for this script are the location and the respective size of the local model, while the obtained output files contain nodes and elements. The size of the local model is designed such that it should cover one neighboring element in-plane additional to damaged ones in case of the intralaminar damage as suggested in earlier work [10]. The reason is that the paths of the matrix and fibre damage growth are unknown in advance. Although it should be noted, that as the displacements from the global model correspond to the displacement load when the failure

criterion was just satisfied, the damage is not expected to evolve outside of these boundaries. As for the interlaminar damage, the local models include only the connector elements detected by the failure criterion as it is expected that the skin-stringer debonding propagates towards the stringer blade, in this buckling shape, transversely to the longitudinal direction. When the damaged regions from the intralaminar and interlaminar damage overlap one local model is created that covers both areas. Only the damaged parts of the panel are included in the local model in order to decrease the computational costs. Thus, the local models contained the skin and the foot of the stringer until the fourth coupling loop where the stringer was also damaged and consequently incorporated into the local models. The only required parameter is the position within the global model. Displacements from the global analysis are utilized as kinematic boundary conditions at the edges of the local model through the submodeling procedure. The same mesh density and material parameters as for the reference model are implemented for the sake of consistency. This means that for the local model the same number (namely four) of cohesive elements per in-plane side of solid element is employed. Intralaminar damage effects are accounted for through the material degradation model by Linde [15].

The damaged local model created based on the global results of the first coupling loop (Fig. 5) is shown in Fig. 6. Matrix damage developed in the region of the stringer, cohesive elements are degraded according to the global model predictions – near the longitudinal edges of the stringer foot. It might be also noticed that some cohesive elements at the edges are not deleted as it might be physically expected. Cohesive elements in Abaqus [29] are prevented from being deleted under pure compression to prevent interpenetration of the surrounding layers. In this case the degradation parameter of this element is equal to 1 and during the recalculation of the global stiffness it corresponds to the fully damaged element.

Coupling loop 1. Local model 2:
(a) matrix degradation
(b) degradation of cohesive elements

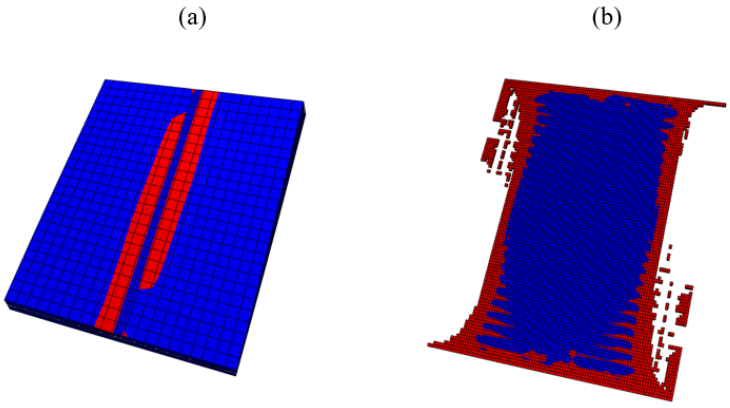

Fig. 6 Coupling loop 1, Local model 2, in red: (a) Matrix damage, (b) Cohesive elements degradation.

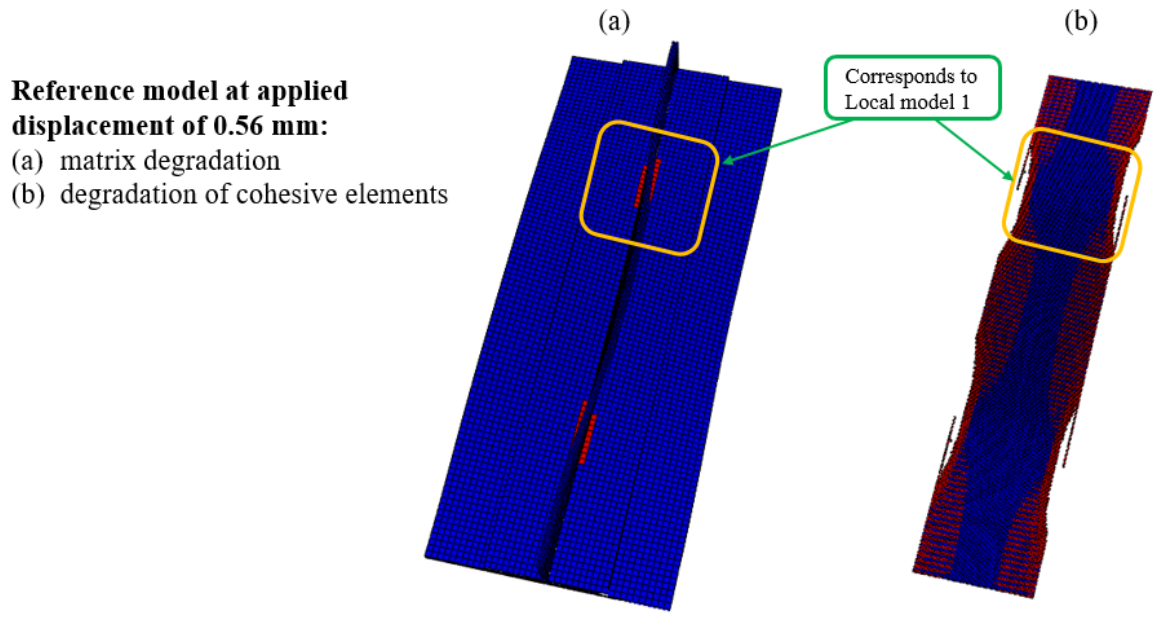

Fig. 7 Reference model, displacement u=0.56 mm, in red: (a) Matrix damage, (b) Cohesive elements degradation.

D. Local-Global Transfer of Updated Properties

Different mesh densities at local and global levels are used. The homogenization-based technique for matrix and fibre damage proposed by Hühne et al. [1] was used to determine equivalent properties corresponding to each global element. In the current studies, these effective material properties are calculated for each laminate layer of a global element independently.

Stiffness degradation of the connector elements is performed using Eq. 12 and applied during the next global analysis step making use of the Abaqus *FIELD option. Hence, the original material properties of the connector elements are used at the global level until the increment at which damage is detected. From that increment, degraded material properties (degraded stiffness) are applied. With an increase of the loading, a degradation of material properties at the global level is performed subsequently.

E. Coupling Results

The load-displacement curves shown in Fig. 8 demonstrate a comparison of the reference model results and of the global-local coupling loops where matrix and fibre damage and debonding between skin and stringer were considered. A good agreement between the reference results and the coupling loops can be observed. After local buckling in both analyses, the coupling curves remain straight until the first failure was predicted. The discrepancy of the first failure prediction between the reference and coupling curves can be explained by the fact that determination of the failure was performed at the global level with a coarse mesh, which again confirms the necessity of a local model with refined mesh

to be examined. During the first coupling loop, the global model is loaded with 0.56 mm of compressive displacement. Both matrix cracking at the stringer basement and debonding onset at the free edge were detected. Based on these results, two local models were created and demonstrated both types of damage initiation and evolution, see Fig. 5 and Fig. 6. The locations of the intralaminar damage and skin-stringer debonding in the reference model at the corresponding applied displacement of 0.56 mm are shown in Fig. 7 with relatively good agreement to the same prediction in the local model. The updated material properties were transferred back to the global level. Here, the coupling load-displacement curve decreased load due to sudden degradation of the properties and ensuing stress redistribution. However, the reference solid model demonstrates a smoother softening behavior which is explained by the fact that the material properties of the reference model are degraded gradually during the numerical analysis. For the coupling simulations, a sudden drop of the load-displacement curve is provoked by the sudden degradation of the material stiffness parameters. The subsequent increase of the compressive displacement up to 0.60 mm demonstrated the evolution of the matrix damage and debonding at both critical areas identified at the first step. The compression was further increased until a displacement of 0.63 mm where due to the debonding growth two local models join into one. Finally, the displacement increase up to 0.67 mm provoked the spreading of fibre and matrix damage across the structure. The panel was severely damaged at that stage, corresponding to a large drop in the load-carrying capacity, see Fig. 8, and final failure occurred.

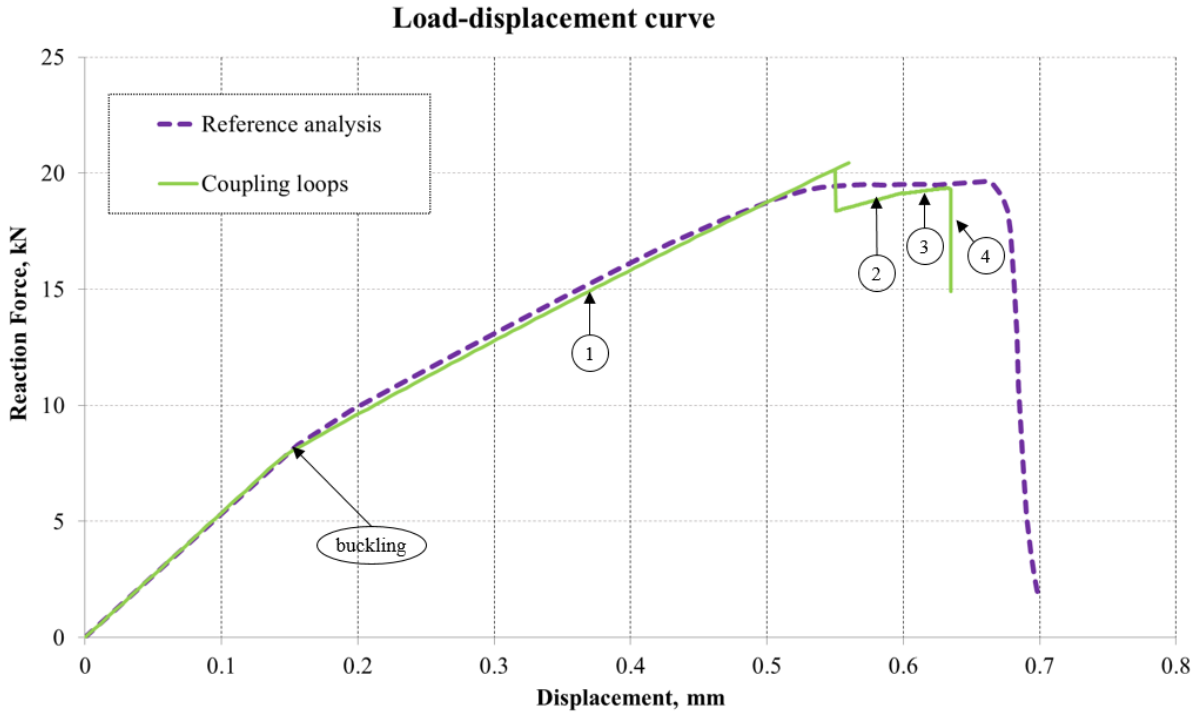

Fig. 8 Load-displacement curve of the coupling and references analyses.

Global, local and reference models analyses were carried out under the same computational characteristics. The total calculation times are 168 s for the first and 265 s for the last global model steps respectively, and 191,084 s for the full 3D

Table 4 Computational characteristics of models.

Model	Number of nodes	Number of elements	Degrees of freedom	Total computational time, s
Reference model	192,136	68,800	463,980	191,084
Global model, 1^{st} coupling loop	756	385	2,331	168
Global model, 4^{th} coupling loop	756	385	2,331	265
Local model 1, 1^{st} coupling loop	40,510	21,608	99,906	23,601
Local model 1, 2^{nd} coupling loop	40,510	21,608	99,906	42,594
Local model 1, 3^{rd} coupling loop	7,750	6,480	23,250	21,816
Local model 1, 4^{th} coupling loop	10,440	8,680	31,320	5,445

reference model. Material nonlinearity is included in both global and reference models. However, the reference model numerical analysis described previously allows for the incremental degradation of the stiffness parameters, whereas the stiffness update in the global model is performed only four times according to the number of steps. It is important to note that the total computational time required for the global-local procedure is the sum of the analysis time of global and local model analysis. It includes four coupling analyses for the global model, with relatively low computational effort, see Table 4 where only global time for the first and last coupling loops are presented to demonstrate the value range. The computational time for local models varies from 23,601 s for the local model of the first coupling step to 42,594 s for the second coupling step. During the third and fourth coupling steps, cohesive damage was recognized as not being significant at the local level and was not accounted for. Hence, the computational time was reduced for local models during the fourth step to 5,445 s for the first local model, for example. It can be concluded that for this test case the computational time of the global-local analysis is comparable with the computational time of the reference model due to relatively large areas of damage. In Table 4, numerical parameters of these models are represented to give an overview of the order of difference between the reference, local and global-local analyses. In this Table the computational time of the first local model is shown for each coupling loop. It is expected that due to the fact that both local models could be calculated independently and, thus, in parallel, only the largest computational time of the two models during the same coupling loop is important.

V. Comparison with Experimental Results

Finally, a comparison of the numerical calculations of the extended global-local approach with existing experimental results is carried out. The chosen specimen was examined within the COCOMAT project in [6] and was denoted as D1 in these studies, see Fig. 9. The global-local method was previously validated for this case considering only matrix and fibre damage modes [1] with some differences in behaviour when reaching the failure load. Following

the observations during the experimental procedure, a separation between skin and stringer also took place. For this reason, it is interesting to compare the experimental results with the coupling calculations including the combination of skin-stringer debonding and intralaminar failure.

Geometric data and the stacking sequence corresponding to skin and stringer and their resulting total thickness are summarized in Table 5. The unidirectional CFRC material IM7/8552 UD was used for manufacturing the skin and the stringer of the panel and FM 300 for the adhesive, see Table 6 for the material properties. The mechanical properties of the adhesive layer were utilized as for the previous analysis; see Table 2, they correspond to the FM 300 material.

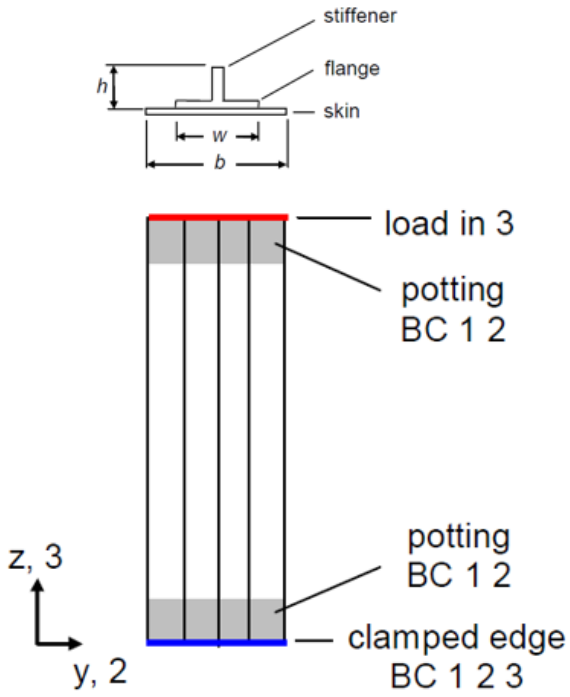

Fig. 9 Geometry of D1 stiffened panel (from [6]).

A. Reference Model

A reference model is created with linear solid elements (C3D8 of Abaqus) utilized for skin and stringer of the composite panel and the nonlinear material degradation model is included in the analysis. The cohesive elements discussed earlier with bilinear traction-separation law are applied to model skin-stringer separation with four cohesive elements per side of one solid element. Mesh convergence studies were performed in order to choose an in-plane solid element length of 1 mm. One element through the thickness represents one composite layer. Finally, the mesh of the reference model consists of 678,800 brick and 198,400 cohesive elements. The first eigenmode is used as an initial imperfection to trigger the postbuckling shape. The geometry and boundary conditions of the composite panel are created with reference to the experimental data presented in Fig. 9. One of the transverse edges is fully clamped at the

Table 5 Geometry data of a D1 stiffened panel (from [6]).

Description	Value
Total length, L (mm)	400
Free length, L_f (mm)	300
Width, b (mm)	64
Stiffener width, w (mm)	32
Stiffener height, h (mm)	14
Ply thickness, t (mm)	0.125
Skin lay-up	$[90, \pm 45, 0]_s$
Stiffener lay-up	$[(\pm 45)_3, 0_6]_s$
Ply thickness, t_{skin} (mm)	1.5
Stringer flange thickness, t_{flange} (mm)	1.5
Stringer web thickness, t_{skin} (mm)	1.0

Table 6 Material data for composite layer of D1 stiffened panel (from [6]).

Stiffness properties	Value
Young's modulus in 1-direction, E_{11} (MPa)	147000
Young's modulus in 2-direction, E_{22} (MPa)	11800
Shear modulus in 12-plane, G_{12} (MPa)	6000
Shear modulus in 31-plane, G_{31} (MPa)	6000
Shear modulus in 23-plane, G_{23} (MPa)	4000
Poisson's ratio, ν_{12}	0.3
Tensile failure stress in 1-direction, X_T (MPa)	2583
Compressive failure stress in 1-direction, X_C (MPa)	1483
Tensile failure stress in 2-direction, Y_T (MPa)	92
Compressive failure stress in 2-direction, Y_C (MPa)	270
Shear failure stress in 12-plane, S_A (MPa)	106
Fracture energy of fiber, G_f (N/mm)	12.5
Fracture energy of matrix, G_m (N/mm)	1.0

end, in all degrees of freedom, except the displacement in the longitudinal direction, are constrained at the opposite edge.

B. Global Model: Linear Elastic Material

The global model consists of 2800 linear shell elements (S4R) with an in-plane element size equal to 4 mm which means 100 elements in longitudinal direction and 909 connector elements for the adhesive layer. The boundary conditions are similar to the reference solid model. The stiffness of the connector elements is degraded consequently during the coupling procedure with regard to the degradation at the local level. The linear elastic material model is defined by means of a user-defined subroutine (UMAT) and the material properties are decreased .

C. Local Models: Material Non-Linearity and Cohesive Debonding

The local models are created with the same mesh density and the same type of solid element (C3D8 of Abaqus) as the reference solid model. The size and position of the local models are defined based on the critical areas observed at the global level.

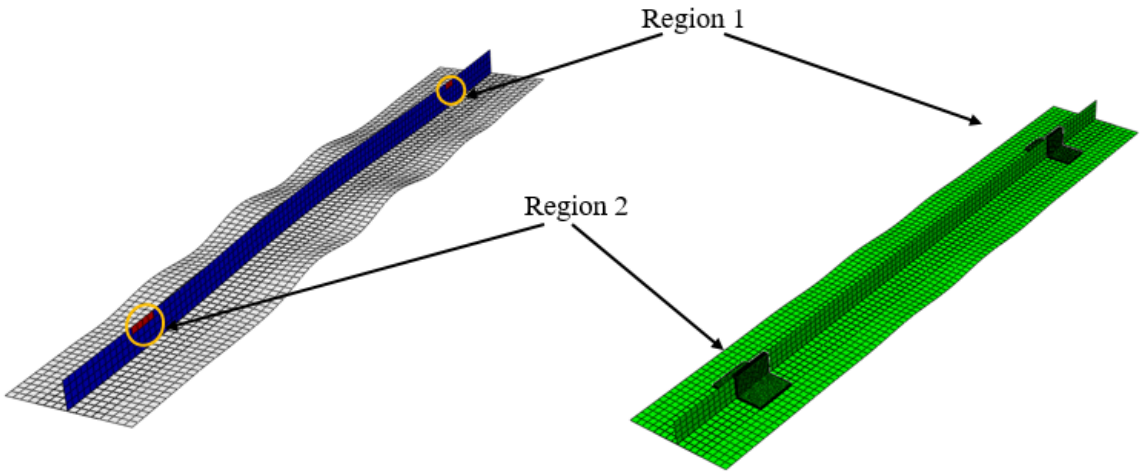

Fig. 10 Iteration 1. Critical global areas for the fibre damage in the blade of the stiffener (left) and overlay plot of two corresponding local models (right) for the intact panel D1.

D. Coupling Results

During the experimental tests, the D1 specimen demonstrated all types of damage instantaneously, such as skin-stringer separation, fiber fracture in the stringer and matrix cracking around the skin-stringer interface [6] not allowing for a proper definition of the damage sequence. The final failure happened due to intralaminar damage near the loaded or clamped edges. In accordance with the experimental results, the numerical analysis of the global-local coupling loops and the reference solid model both demonstrated sudden initiation and evolution of the damage in the blade of the stiffener, and separation between skin and stringer together with extensive matrix damage at the foot of the stringer.

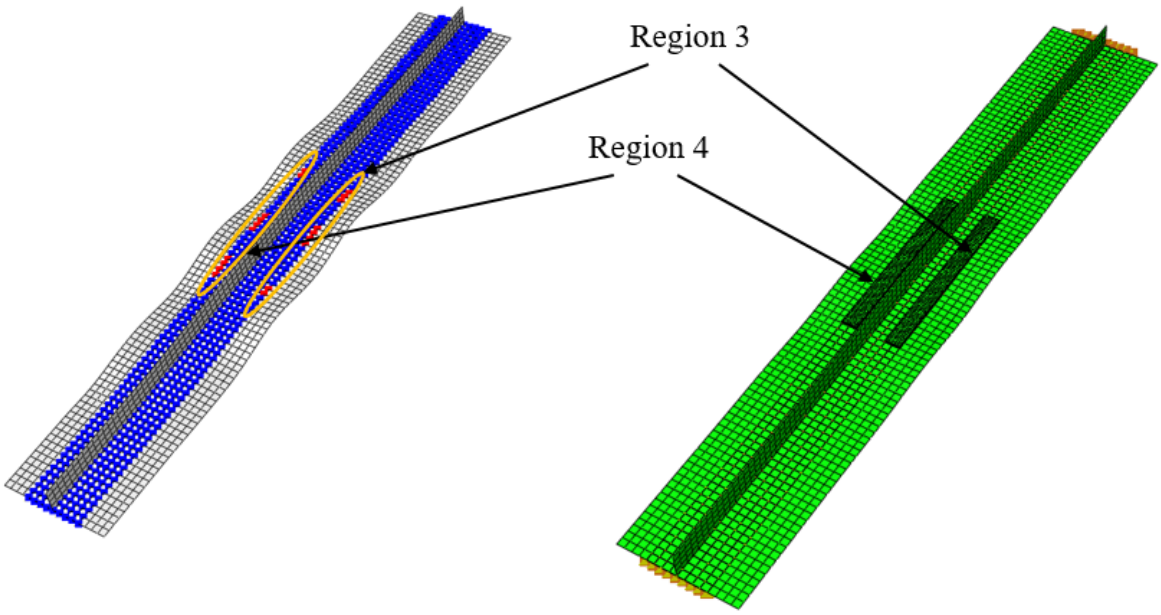

Fig. 11 Iteration 1. Critical global areas for the skin-stringer debonding (left) and overlay plot of two corresponding local models (right) for the intact panel D1.

One coupling loop at the displacement load level of 1.9 mm was performed and it was observed that the damage had already started at a slightly lower level. After three iterations of coupling loops, the simulation of the damage propagation in the global model resulted in a final collapse of the panel. At the displacement level of around 1.89 mm, the fiber damage started symmetrically at the stringer blade in the regions close to the potting system. Two local models were created that account for the material damage evolution in the stringer, corresponding to Regions 1 and 2 in Fig. 10. Approximately at the same load level, the debonding between skin and stringer were detected, see Fig. 11. The evolution of the damage in blades of the stringer after the second iteration required an increase of the local models' sizes which is illustrated in Fig. 12. The intralaminar damage in the reference model shown in Fig. 13 also occurred in two areas similarly to the global model predictions. Although it should be noted that the damage in the blade of the reference model developed differently than in the local models. This difference might be explained by the submodeling procedure which only transfers displacements without satisfying the equilibrium requirements. As the damage started at both sides of the stringer, two types of local models creation approaches were compared: one full local model covering both sides and two separate local models. The aim was to choose the computationally most effective approach without important loss in accuracy of the degradation prediction. Finally, it was concluded that two separate local models, located as shown in Fig. 11 symmetrically to the stringer and covering the damaged Regions 3 and 4, are sufficiently accurate. The damage in cohesive elements from these local models is demonstrated in Fig. 14 and agrees

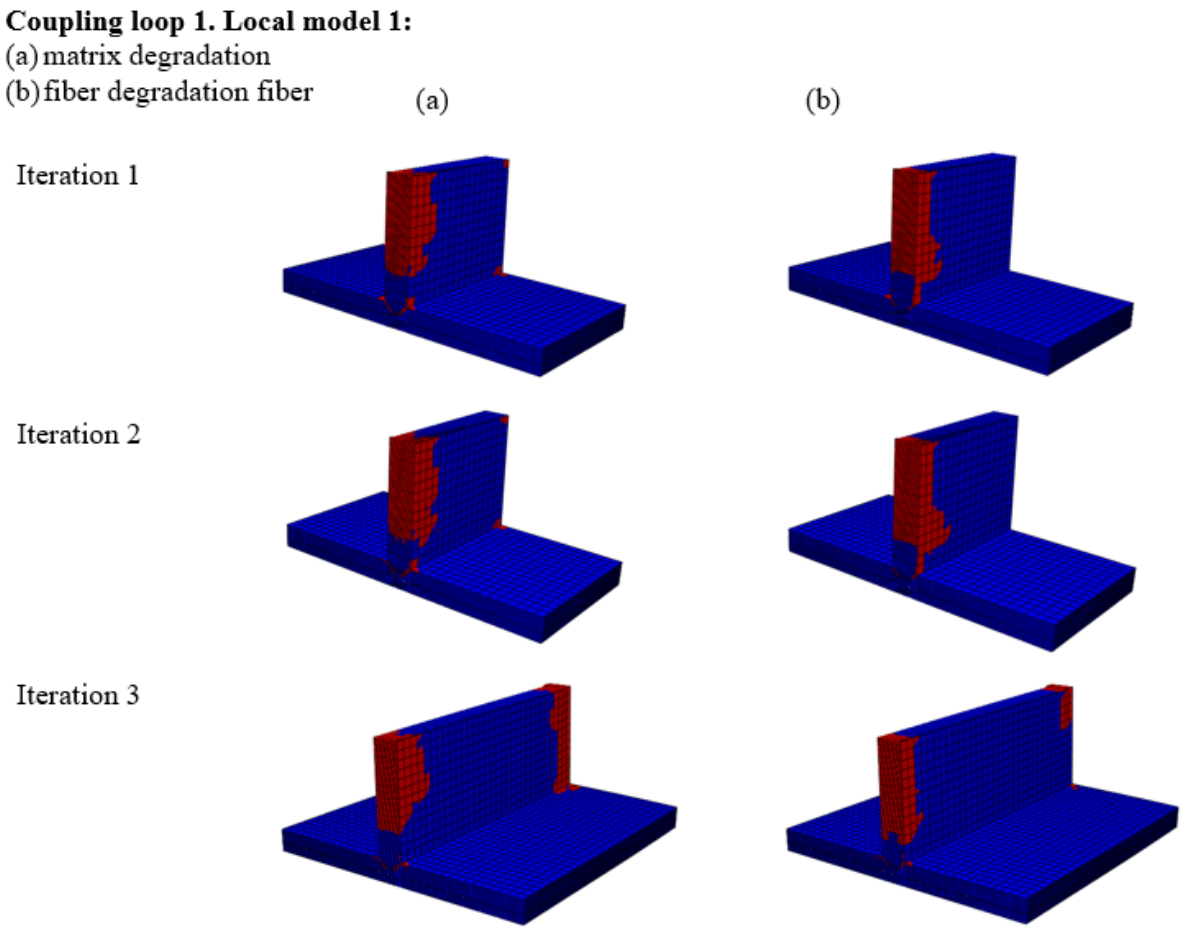

Fig. 12 Matrix and fiber damage of local model 1 for the intact panel D1 (Iterations 1–3) In red: new local damage.

sufficiently well with the damage in the reference model at the displacement of 1.9 mm. The load-displacement curves for three experimental results [14] and numerical simulations obtained from the coupling procedure and reference solid model are shown in Fig. 15. The initial structural stiffness of the numerical simulations correlates well with one of the experimental measurements, while the slight discrepancy with the other two experimental results could be explained by the applied material properties that were suggested by Orifici et al. [14]. The developed global-local strategy accords to experimental solution in terms of the location and sequence of detected damage events as well as in the final collapse.

Similarly to the previous case, numerical parameters of the global, local and reference models are presented in Table 7. The computational time is shown for the first local model that was created to account for the damage in the blade of the stringer, see Fig. 10, as the maximum computational time during the iteration loops for local models. Thus, the total computational time to complete the global-local coupling analysis took 964,806 s, whereas for the full reference model this time was 1,932,780 s. The decrease of the computational time by around 50% obtained by the global-local simulation compared to the full 3D modeling is a significant achievement of the developed method.

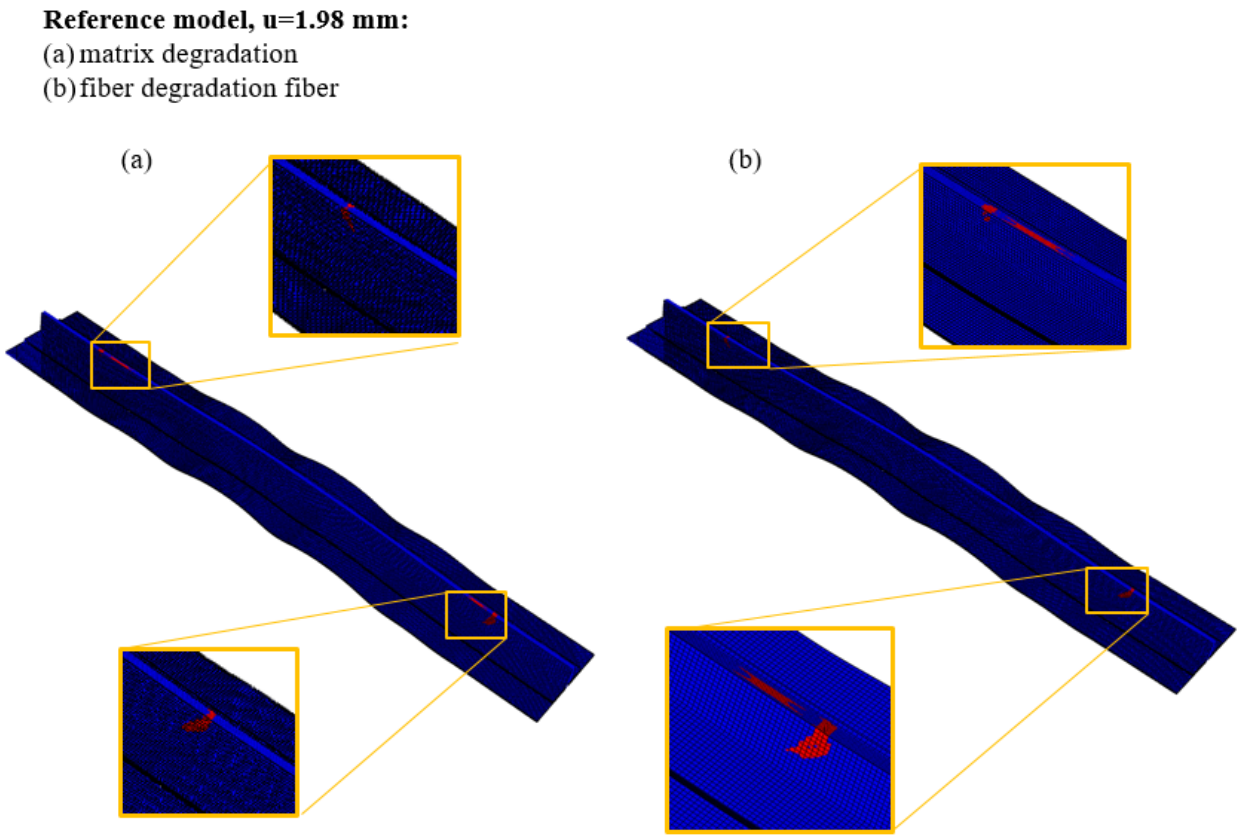

Fig. 13 Matrix and fiber damage of reference model for the intact panel D1 at the displacement of 1.9 mm.

The comparison of the coupling method results with experimental observations and the reference solid model analysis revealed, that the coupling method was able to predict realistic damage modes and to account for their growth. The occurrence of fiber damage in the blade of the stringer was predicted as in the earlier global-local analysis in [1] including intralaminar damage only, but unlike the results in [1], in the current simulations the fiber damage propagated over a considerably larger region during the global-local analysis. This increase of the damaged area can be attributed to the consideration of the skin-stringer debonding in the current analysis and the corresponding stress redistribution over the structure. The results of the global-local coupling analysis compare reasonably well with the experimental results; there is a deviation of less than 10% in the prediction of the final failure load.

VI. Conclusion

In this paper, a two-way loose coupling approach for progressive failure analysis was presented for the combination of intralaminar and debonding damage modes. Inclusion of both damage mechanisms in the global-local strategy allows for observation of progressive damage evolution similar to that shown in actual structures. The creation of separate global and local models allows the evolution of damage in the local models to be considered, while the material linearity

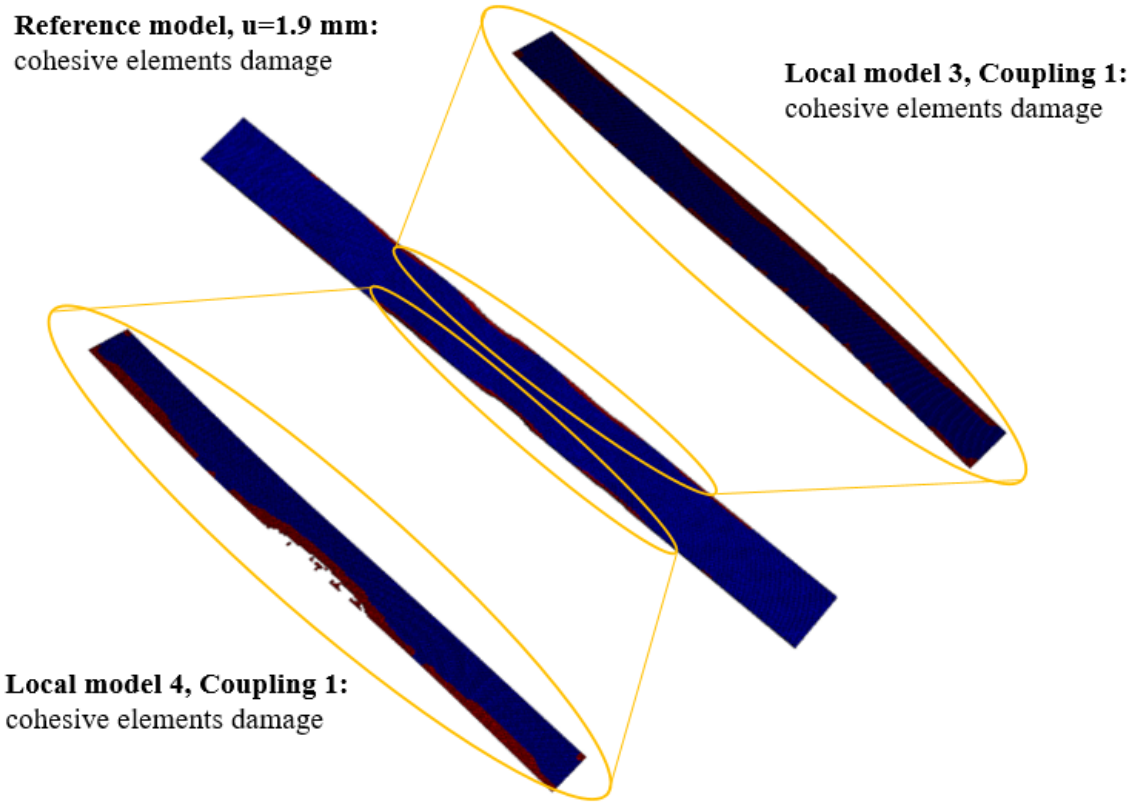

Fig. 14 Cohesive element damage of reference model and local models 3 and 4 for the intact panel D1 at the displacement of 1.9 mm.

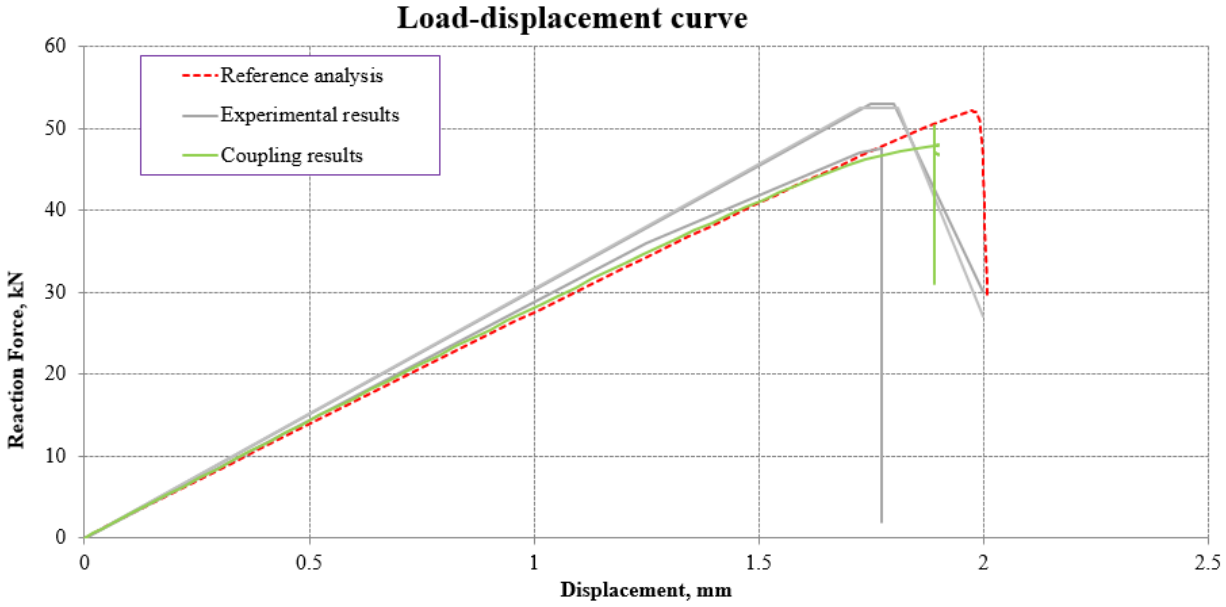

Fig. 15 Load-displacement curve of the D1 stiffened panel.

Table 7 Computational characteristics of models for the intact panel D1.

Model	Number of nodes	Number of elements	Degrees of freedom	Total computational time, s
Reference model	1,166,160	857,600	4,272,111	1,932,780
Global model, 1^{st} iteration	3,030	3,709	22,878	323
Global model, 2^{nd} iteration	3,030	3,709	22,878	742
Global model, 3^{rd} iteration	3,030	3,709	22,878	709
Global model, 4^{th} iteration	3,030	3,709	22,878	2089
Local model 1, 1^{st} iteration	82,198	54,144	241,419	271,937
Local model 1, 2^{nd} iteration	82,198	54,144	241,419	268,128
Local model 1, 3^{rd} iteration	108,918	72,192	396,039	420,878

and standard mesh with shell elements of the global model ensures a fast computational time. One of the advantages of using separate models is the fact that the position of the local model can be easily adjusted based on the increase of the critical area at the global level. The studies performed in particular assess the effect of skin-stringer debonding growth on the global panel failure while including intralaminar damage (matrix and fibre damage). The local models obtain interpolated displacements as boundary conditions from the global model through a submodeling procedure. In turn, the global model uses the decreased material properties transferred from the local model to simulate the degradation of the material at the global level and can thus carry out a progressive failure analysis.

The method was illustrated for one-stringer composite panels. First, a numerical simulation of the coupling procedure was compared with the results of a reference model with 3D elements. For another test case, the numerical calculations of the two-way coupling approach were compared with existing experimental results. A reasonable agreement for load-displacement curves between reference model and global-local coupling analysis in the first case, and between experimental data and the coupling approach in the second case was obtained. A reduction of about 50% in computational time achieved by the global-local method demonstrates a significant potential for this approach. The global-local analysis for debonding damage can be further enhanced by also considering the mixed-mode damage evolution in the debonding analysis.

VII. Acknowledgments

The research leading to these results has received funding from European Union's Horizon 2020 research and innovation program (FULLCOMP/2015-2019) under Marie Sklodowska-Curie actions grant agreement number 642121. The provided financial support is gratefully acknowledged by the authors. Paul M. Weaver would like to thank Science Foundation Ireland for funding VARICOMP under its Research Professor scheme.

References

[1] Hühne, S., Reinoso, J., Jansen, E., and Rolfes, R., "A two-way loose coupling procedure for investigating the buckling and damage behaviour of stiffened composite panels," *Composite Structures*, , No. 136, 2016, pp. 513–525. doi:10.1016/j.compstruct.2015.09.056.

[2] Loehnert, S., and Belytschko, T., "A multiscale projection method for macro / microcrack simulations," *International Journal for Numerical Methods in Engineering*, , No. 71, 2007, pp. 1466–1482. doi:10.1002/nme.2001.

[3] Labeas, G. N., Belesis, S. D., Diamantakos, I., and Tserpes, K. I., "Adaptative Progressive Damage Modeling for Large-scale Composite Structures," *International Journal of Damage Mechanics*, Vol. 21(3), 2012, pp. 441–62. doi:10.1177/1056789511400928.

[4] Chrupalla, D., Kreikemeier, J., Berg, S., Kärger, L., Doreille, M., Ludwig, T., Jansen, E., Rolfes, R., and Kling, A., "A loose coupling multiscale approach for the detailed analysis of the influence of critical areas on the global behaviour of composite structures," *Computers, Materials and Continua*, Vol. 32, No. 3, 2012, pp. 159–176. doi:10.3970/cmc.2012.032.159.

[5] Reinoso, J., Blázquez, A., Estefani, A., París, F., Cañas, J., Arévalo, E., and Cruz, F., "Composites : Part B Experimental and three-dimensional global-local finite element analysis of a composite component including degradation process at the interfaces," *Composites Part B*, Vol. 43, No. 4, 2012, pp. 1929–1942. doi:10.1016/j.compositesb.2012.02.010.

[6] Orifici, A. C., Ortiz, I., Alberdi, D. Z., Thomson, R. S., and Bayandor, J., "Compression and post-buckling damage growth and collapse analysis of flat composite stiffened panels," *Composites Science and Technology*, Vol. 68, No. 15-16, 2008, pp. 3150–3160. doi:10.1016/j.compscitech.2008.07.017.

[7] Faggiani, A., and Falzon, B. G., "Optimization Strategy for Minimizing Damage in Postbuckling Stiffened Panels," *AIAA Journal*, Vol. 45, No. 10, 2007, pp. 2520–2528. doi:10.2514/1.26910.

[8] Gendre, L., Allix, O., Gosselet, P., and Francois, C., "Non-intrusive and exact global / local techniques for structural problems with local plasticity," *Comput Mech*, Vol. 44, 2009, pp. 233–245. doi:10.1007/s00466-009-0372-9.

[9] Vescovini, R., Dávila, C. G., and Bisagni, C., "Failure analysis of composite multi-stringer panels using simplified models," *Composites Part B*, Vol. 45, No. 1, 2013, pp. 939–951. doi:10.1016/j.compositesb.2012.07.030.

[10] Akterskaia, M., Jansen, E., Hühne, S., and Rolfes, R., "Efficient progressive failure analysis of multi-stringer stiffened composite panels through a two-way loose coupling global-local approach," *Composite Structures*, Vol. 183, 2018, pp. 137–145. doi:10.1016/j.compstruct.2017.02.011.

[11] Akterskaia, M., Jansen, E., Hallett, S., Weaver, P., and Rolfes, R., "Analysis of skin-stringer debonding in composite panels through a two-way global-local method," *Composite Structures*, 2018. doi:10.1016/j.compstruct.2018.06.064.

[12] Degenhardt, R., Kling, A., Klein, H., Hillger, W., Goetting, H. C., Zimmermann, R., and Rohwer, K., "Experiments on buckling and postbuckling of thin-walled CFRP structures using advanced measurement systems," *International Journal of Structural Stability and Dynamics*, Vol. 7, No. 2, 2007, pp. 337–358. doi:10.1142/S0219455407002253.

[13] Zimmermann, R., Klein, H., and Kling, A., "Buckling and postbuckling of stringer stiffened fibre composite curved panels – Tests and computations," *Composite Structures*, Vol. 73, 2006, pp. 150–161. doi:10.1016/j.compstruct.2005.11.050.

[14] Orifici, A. C., Thomson, R. S., Degenhardt, R., Kling, A., Rohwer, K., and Bayandor, J., "Degradation investigation in a postbuckling composite stiffened fuselage panel," *Composite Structures*, Vol. 82, 2008, pp. 217–224. doi:10.1016/j.compstruct.2007.01.012.

[15] Linde, P., Pleitner, J., Boer, H. D., and Carmone, C., "Modelling and simulation of fibre metal laminates," *ABAQUS Users' Conference*, 2004, pp. 421–439.

[16] Pinho, S. T., Dávila, C. G., Camanho, P. P., Iannucci, L., and Robinson, P., "Failure Models and Criteria for FRP Under In-Plane or Three-Dimensional Stress States Including Shear Non-linearity," *Nasa/Tm-2005-213530*, , No. NASA/TM-2005-213530, 2005, p. 68. doi:NASA/TM-2005-213530.

[17] Pinho, S. T., Vyas, G. M., and Robinson, P., "Response and damage propagation of polymer-matrix fibre-reinforced composites: Predictions for WWFE-III Part A," *Journal of Composite Materials*, Vol. 47, No. 20-21, 2013, pp. 2595–2612. doi:10.1177/0021998313476972.

[18] Hinton, M. J., Kaddour, A. S., and Soden, P. D., "A comparison of the predictive capabilities of current failure theories for composite laminates , judged against experimental evidence," *Composites Science and Technology*, Vol. 62, 2002, pp. 1725–1797. doi:10.1016/S0266-3538(02)00125-2.

[19] Kaddour, A. S., and Hinton, M. J., "Maturity of 3D failure criteria for fibre-reinforced composites: Comparison between theories and experiments: Part B of WWFE-II," *Journal of Composite Materials*, Vol. 47, 2013, pp. 925–966. doi:10.1177/0021998313478710.

[20] Kaddour, A. S., Hinton, M. J., and Soden, P. D., "A comparison of the predictive capabilities of current failure theories for composite laminates : additional contributions," Vol. 64, 2004, pp. 449–476. doi:10.1016/S0266-3538(03)00226-4.

[21] Kaddour, A. S., Hinton, M. J., Smith, P. A., and Li, S., "Mechanical properties and details of composite laminates for the test cases used in the third world-wide failure exercise," *Journal of Composite Materials*, Vol. 47, No. 20-21, 2013, pp. 2427–2442. doi:10.1177/0021998313499477.

[22] "Review of Degradation Models for Progressive Failure Analysis of Fiber Reinforced Polymer Composites," *Applied Mechanics Reviews*, Vol. 62, No. 1, 2009, p. 010801. doi:10.1115/1.3013822.

[23] Forghani, A., Shahbazi, M., Zobeiry, N., Poursartip, A., and Vaziri, R., "An overview of continuum damage models used to simulate intralaminar failure mechanisms in advanced composite materials," *Numerical modelling of failure in advanced composite materials*, 2015, pp. 151–173. doi:10.1016/B978-0-08-100332-9.00006-2.

[24] Turon, A., Camanho, P. P., and Costa, J., "An engineering solution for mesh size effects in the simulation of delamination using cohesive zone models," *Engineering Fracture Mechanics*, Vol. 74, 2007, pp. 1665–1682. doi:10.1016/j.engfracmech.2006.08.025.

[25] Wagner, W., and Balzani, C., "Simulation of delamination in stringer stiffened fiber-reinforced composite shells," *Computers and Structures*, Vol. 86, 2008, pp. 930–939. doi:10.1016/j.compstruc.2007.04.018.

[26] Harper, P. W., and Hallett, S. R., "Cohesive zone length in numerical simulations of composite delamination," *Engineering Fracture Mechanics*, Vol. 75, 2008, pp. 4774–4792. doi:10.1016/j.engfracmech.2008.06.004.

[27] Benzeggagh, M. L., and Kenane, M., "Measurement of Mixed-Mode Delamination Fracture Toughness of Unidirectional Glass / Epoxy Composites With Mixed-Mode Bending Apparatus," *Composites Science and Technology*, Vol. 56, 1996, pp. 439–449. doi:10.1016/0266-3538(96)00005-X.

[28] Lauterbach, S., Orifici, A. C., Wagner, W., Balzani, C., Abramovich, H., and Thomson, R., "Damage sensitivity of axially loaded stringer-stiffened curved CFRP panels," *Composites Science and Technology*, Vol. 70, No. 2, 2010, pp. 240–248. doi:10.1016/j.compscitech.2009.10.013.

[29] Abaqus, "Abaqus Documentation, Abaqus 6.14 Documentation. Dassault systemes. 6.14 edn." , No. V, 2017, pp. 1–172.